Nanofibrous material from hyaluronan derivatives preserving fibrous structure in aqueous environment

Nanofibrous material from hyaluronan derivatives preserving fibrous structure in aqueous environment

Kristýna Skuhrovcová[a,b], Adela Kotzianová[a,*], Lenka Bardonová[a,c], Ondřej Židek[a], Evgeniy Toropitsyn[a], Hana Vágnerová[a], Aneta Čápová[a,d], Kateřina Dostálová[a], Martina Hermannová[a], Marek Pokorný[a], Vladimír Velebný[a]

[a]*Contipro a.s., Dolní Dobrouž 401, 561 02, Czech Republic*

[b]*Centre of Polymer Systems, Tomas Bata University in Zlín, TŽda Tomaže Bati 5678, 760 01 Zlín, Czech Republic*

[c]*Nanotechnology Centre, Energy and Environmental Technology Centre, VŠB-Technical University of Ostrava, 17, Listopadu 2172/15, 708 00 Ostrava, Czech Republic*

[d]*Department of Biological and Biochemical Sciences, Faculty of Chemical Technology, University of Pardubice, Studentska 573, 532 10 Pardubice, Czech Republic*

[*]*Corresponding authors: skuhrovcova@contipro.com (K. Skuhrovcová), kotzianova@contipro.com (A. Kotzianová), bardonova@contipro.com (L. Bardoňová), Ondřej. Zidek@contipro.com (O. židek), toropitsyn@contipro.com (E. Toropitsyn), Hana.Vagnerova@contipro.com (H. Vágnerová), capova@contipro.com (A. Čápová), dostalova@contipro.com (K. Dostálová), hermannova@contipro.com (M. Hermannová), pokorny@contipro.com (M. Pokorný), velebny@contipro.com (V. Velebný).*

ABSTRACT

Nanofibrous materials produced from natural polymers have wide range of potential uses in regenerative medicine. This paper focuses on preparation of nanofibrous layers produced from intentionally hydrophobized derivatives of hyaluronan, which is known for its ability to promote wound healing. This structural modification of hyaluronan expands the range of potential uses of this promising material, which is otherwise limited due to the hydrophilic nature of hyaluronic acid. The aim of this research was preparation of nanofibrous material that would retain its fibrous structure and dimensional stability even after getting into contact with an aqueous medium, which is impossible to achieve with layers composed solely of native hyaluronan. As a result, such material would be able to retain its breathability and good mechanical properties when both dry and wet. Furthermore, all prepared materials were proved non-toxic for cells. This self-supporting nanofibrous matrix can be used as a scaffold, or porous wound dressing.

Keywords: Hyaluronic acid, hydrophobized hyaluronan, nanofibers, crosslinking, swelling

Abbreviations: BSA, Bovine serum albumin; BTH, Bovine testicular hyaluronidase; CO_2, carbon dioxide; DMAP, 4-dimethylaminopyridine; DMEM, Dulbecco's Modified Eagle Medium; DS, degree of substitution; DW, distilled water; F-HA, 3-(2-furyl)acrylic acid derivative of sodium hyaluronate; ECM, extracellular matrix; HA, hyaluronan; HaCaT, Human Immortalized Keratinocytes; IPA, 2-propanol; L-HA, lauroyl derivative of sodium hyaluronate; MTT, 3-(4,5-dimethylthiazol- 2-yl)-2,5-diphenyl-tetrazolium bromide; NaCl, sodium chloride; NHDF, Normal Human Dermal Fibroblasts; PBS, phosphate buffered saline; PEO, poly(ethyleneoxide); RH, relative humidity; SEM, Scanning electron

microscopy; SpHyl, hyaluronan lyase from Streptococcus Pneumoniae; TEA, triethylamine; UV, ultraviolet.

1. Introduction

Hyaluronan (HA) has been recently gaining more attention in wound dressing development due to its natural presence in the extracellular matrix (ECM) and its role in the inflammation and proliferation stages of wound healing. HA is currently clinically used in wound dressings (**Longinotti, 2014**), skin substitutes (**Debels & Hamdi, 2015**), joint lubricants (**Snetkov et al., 2019**), and various connective tissue replacements. Hyaluronan is an anionic linear polysaccharide with a repeating unit consisting of D-glucuronic acid and N-acetyl-D-glucos-amine linked by alternating $\beta(1 \rightarrow 4)$ and p$(1 \rightarrow 3)$ glycosidic bonds. HA is naturally occurring and plays an important role in processes such as tissue hydration and wound healing (**Dicker et al., 2014**). Moreover, due to its biocompatibility, biodegradability, and nontoxicity (Necas et al., 2008), HA is a promising material with numerous potential applications in medicine. Native HA is highly hydrophilic and soluble in water, which makes bandages prepared from native HA inapplicable in medicinal practice, because hyaluronan is dissolved immediately. However, the issue of high solubility can be addressed by covalently cross-linking HA. Published methods include processes based on enzymatic reactions (**Dvorakova et al., 2014**), photochemistry (**Bobula et al., 2015**), and the use of chemical cross-linking agents such as polyvalent hydrazides (**Vercruysse et al., 1997**), glutaraldehyde, divinyl sulfone, and carbo-diimides (**Collins & Birkinshaw, 2007, 2008**). Another option is to chemically modify HA with hydrophobic side groups, such as long acyl chains (**Creuzet et al., 2006; Finelli et al., 2014; Huerta-Angeles et al., 2014; Smejkalova et al., 2012**) or octenyl succinic anhydride (**Een-schooten et al., 2012**). These hydrophobized derivatives could find use in applications that need to be used for long periods of time to be effective, such as wound dressings. These materials can also be modified into various forms. In nanofibrous materials, these derivatives can largely replace synthetic polymers and further enhance their biocompatibility and bioactivity.

Both synthetic and natural polymers are used as essential materials for the preparation of nanofibrous materials. Nowadays these materials are widely used in biomedicine and the areas of their application include, for example, tissue engineering, drug delivery tissue replacement, and wound healing (**Miguel et al., 2018**). The use of nanofibrous materials is particularly beneficial in topical applications, i.e. in treating skin injuries - the structure of nanofibrous materials resembles the fibrous structure formed by naturally occurring collagen commonly present in the extracellular matrix (**Sill & von Recum, 2008**). Nanofibers, usually in the form of thin layers, can be prepared by electrospinning from a wide variety of synthetic and natural polymers. Self-supporting nanofibrous structures, e.g. in the form of a plaster, can be immediately applied to a wound where they provide necessary conditions for proper healing. Most of the nanofibrous wound dressings that have been developed so far are made from synthetic polymers (polycaprolactone, polyurethane, polylactic acid, etc.), to which natural polymers (collagen, hyaluronic acid, gelatin, chitosan, etc.) are added as additives (**Almasian et al., 2020; Fang et al., 2019; He et al., 2020; Liu et al., 2019; Unalan et al., 2019**). In these applications, the base synthetic polymer performs primarily a mechanical function, while the added natural polymer exhibits biological activity.

The aim of this study was to prepare nanofibrous materials from two hydrophobized derivatives of hyaluronic acid with potential applications in the biomedical area, where the stability in aqueous solutions and gradual degradation of the polymer matrix is required (e.g. drug release, wound healing or scaffolds). The first of the two derivatives, a lauroyl derivative, previously reported as safe for implantation into mammal organisms, but never electrospun (**Chmelar et al., 2019**), containing chemically attached fatty lauric acid in its structure. And the second, crosslinkable furanyl derivative,

previously reported as suitable for nanofabrication and capable of keeping fibrous structure while wet (**Huerta-Angeles et al., 2016**). This work was focused on suitable parametrization of electrospinning process for preparation of selfsupporting composite nanofibrous layers from both derivatives. All materials were compared in between. It is expected to prepare such a material that will be mechanically resistant to weak stressing and at the same time will not significantly change its properties and parameters in contact with a water-based fluid. From a biological point of view, the effect of the material on cell viability, its behavior in direct contact with cell cultures, the promotion of cell proliferation and the degradation profile in the presence of the hyaluronidase enzyme were studied. The combination of two derivatives with specific properties should bring a whole new material with synergically improved properties for various medicinal applications.

2. Experimental

2.1. Material

The lauroyl derivative of sodium hyaluronate (L-HA, 350 kDa, 65-80% degree of substitution, Contipro a.s.) was prepared by the esterification of OH groups on a sodium hyaluronate (HA) backbone and by the acylation of HA with a symmetric lauric acid anhydride (**Smejkalova et al., 2012**). In short, HA was first dissolved in distilled water (DW), then triethylamine and the catalyst N,N-dimethylaminopyridine were added. After 1 h of mixing, the solution was diluted with tetra-hydrofuran and further homogenized. Next, the symmetric anhydride was added. At the end of the reaction, the mixture was diluted with 50% 2-propanol (IPA), and a saturated sodium chloride solution was subsequently added. The product was precipitated with absolute 2-propanol, washed, decanted, and dried for 48 h at 40 °C (**Huerta-Angeles et al., 2014**).

The preparation of the 3-(2-furyl)acrylic acid derivative of sodium hyaluronate (F-HA, 100 kDa, 5% degree of substitution, Contipro a.s.) has been described in detail in (**Huerta-Angeles et al., 2016**). In short, HA was dissolved in DW, then IPA, triethylamine (TEA), and 4-dimethy-laminopyridine (DMAP) were added. Once a clear solution was obtained, the anhydride was added to it; the reaction took place over 2 h at room temperature. The product was isolated by precipitation with DW containing NaCl and washed out with DW and IPA. The obtained white precipitate was decanted and then dried at 40 ° C for at least 24 h.

Solutions for electrospinning were prepared as follows. The L-HA solution consisted of L-HA and poly(ethylene) oxide (PEO, 400 kDa, Sigma Aldrich) dissolved in IPA and DW (3:2 ratio). The concentration of the solution was 3% w/w. The ratio of the two polymers was 90:10 L-HA:PEO. The F-HA solution consisted of F-HA and PEO dissolved in DW. The concentration of the solution was 7% w/w. The ratio of the two polymers was 90:10 F-HA:PEO. Solutions for the spinning of the L-HA/F-HA_1, L-HA/F-HA_2, and L-HA/F-HA_3 samples consisted of L-HA, FHA, and PEO dissolved in IPA and DW (1:1 ratio). The concentration of each of the solutions was 3% w/w. The L-HA:F-HA:PEO ratios were 75:20:5 for L-HA/F-HA_1, 48:48:4 for L-HA/F-HA_2, and 20:75:5 for L-HA/F-HA_3. All solutions were stirred for 12 h at room temperature before being used for electrospinning.

2.2. Methods

2.2.1. Electrospinning

The nanofibrous layers were spun using the 4SPIN LAB device (Contipro a.s.). To achieve high productivity and homogeneity of nanofibrous layers, a linear needleless emitter and a rotating collector ((37 x 25) cm^2) were used. The distance between the electrodes was set to 18-20 cm. Rotational speed was set to 100 rpm. Applied voltage ranged from 54 kV to 60 kV, feed rate ranged from 150 to 350 µL/min. Each layer was spun for as long as necessary to achieve the target weight-to-area ratio of 7-10 g/m^2 (about 60-90 min). Silicon paper was used as the substrate, and the nanofibrous layers were peeled off before being analyzed.

2.2.2. Cross-linking of nanofibrous layers

After being electrospun, nanofibrous layers containing F-HA were cross-linked using UV radiation (λ = 302 nm; 350 µJ/cm^2) (**Fig. 1**). A UVP CL-1000 (Fisher Scientific) ultraviolet crosslinker was used for this purpose. The layers were cross-linked for 60 min. All subsequent analyses were performed on cross-linked layers.

2.2.3. Quantification of organic residues

The residual concentration of 2-propanol was determined by gas chromatography using a headspace autosampler and a mass spectrometer detector (Agilent Technologies). The nanofibrous layer sample to be analyzed (10 mg) was inserted into a vial, to which 2 ml of water and 0.1 ml of our standard in-house solution (tert-butanol, 0.1 mg/ml in water) were then added. After its equilibration (shaking at 90 °C, 60 min), the sample was injected into a DB-624-UI column (Agilent J&W GC Columns), and the concentration of 2-propanol (% w/w) was determined.

2.2.4. Scanning electron microscopy

The morphology of the prepared nanofibrous layers was studied with a Zeiss Ultra Plus scanning electron microscope (ZEISS, Germany) - first after the layers were electrospun and again after they were subjected to swelling tests. The nanofibrous layers were coated with a very thin layer of Au/Pd (80/20) in a Leica EM ACE600 sputter coater (Leica, Germany) to prepare them for the SEM analysis.

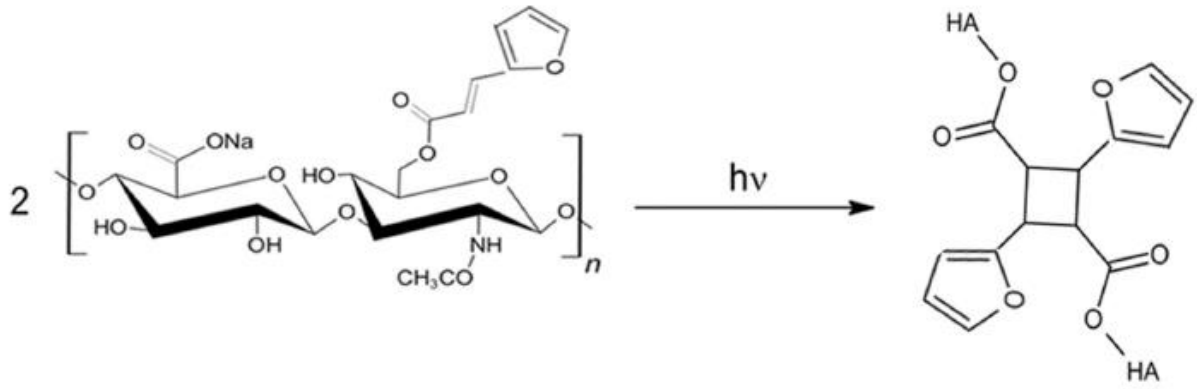

Fig. 1. Cycloaddition reaction during crosslinking of F-HA derivative.

Images were acquired using an InLens SE detector; the working distance ranged from 2.6 mm to 4.0 mm, and the pressure was approximately 10^{-4} Pa. Fiber diameters were assessed manually from images with a magnification of 5000 x; 50 fibers were assessed for each sample.

2.2.5. Thickness measurement and determination of weight-to-area ratios

The weight-to-area ratios of the prepared layers were determined by taking (2 x 2) cm^2 samples from the nanofibrous layers and weighing them. The weight-to-area ratio was calculated as a ratio of sample weight to sample area. Layer thickness was determined using a VL-50 (Mitutoyo) machine for contact measurement of thickness. Each (2 x 2) cm^2 sample was measured at five points (one in each corner and one in the center). A total of 18 samples were measured from each nanofibrous layer. The samples were subsequently used for the analysis of swelling behavior.

2.2.6. Mechanical properties

The mechanical properties of the nanofibrous layers were measured using a DHR-3 rheometer equipped with a dynamic mechanical accessory with a humidity chamber (TA Instruments). Five (1 x 2) cm^2 samples were measured from each nanofibrous layer. The stress-strain curves of the samples were measured in a humidity chamber at a temperature of 37 ° C and a relative humidity of 0%, 50%, and 95%. The tensile test was set to begin only after equilibrium was reached (samples were conditioned for at least 15 min). After samples conditioning, stress, which increased in consequence of temperature and humidity changes, was offset (equilibrated) to zero (initial stress at the beginning of the measurement = 0 Pa). All measurements were conducted at constant linear rate 20 µm/s. The relation between stress and strain was evaluated, including calculation of Young's modulus, ultimate tensile strength and strain at break values.

2.2.7. Swelling behavior

To evaluate the swelling behavior of the prepared nanofibrous layers, (2 x 2) cm^2 samples were individually placed in Petri dishes, to which 7 ml of a phosphate buffer solution (PBS, pH 7.4) were added. Three samples were swelled for each tested nanofibrous layer and for each of the swelling times. The samples were incubated at 37 °C for 1, 3, 8, 24, 48, and 72 h. The samples were then removed from the PBS and gently dried using filter paper and weights. The swelling ratio was calculated according to the following equation:

$$\text{Swelling ratio } (\%) = \frac{m_{wet} - m_{dry}}{m_{dry}} \times 100\%$$

where m_{wet} [g] is the weight of a wet sample and m_{dry} [g] is the weight of a dry sample. As the main advantage of nanofibrous layers consists in their structure, specifically in their very large active area and porosity, the morphology of the layers after swelling was also studied. After the swelling test, the samples were placed into an incubator to dry out (at 37 °C), and their SEM images were taken.

2.2.8. In vitro degradation of nanofibrous layers

In vitro degradation experiments (n = 3 per composition) were performed at 37 °C in 0.01 M sodium acetate buffer pH 5.3 containing BSA (0.5 mg ml^{-1}) and 0 or 30 IU ml^{-1} of bovine testicular hyaluronidase (BTH). Sample (10 ± 0.5 mg) was weighed into the degradation vessel and the degradation solution was added (1 ml). The degradation solution was replaced at predetermined time intervals with the fresh one and stored at 4-8 ° C till HA derivatives quantification. The amount of released HA derivatives was quantified by enzymatic degradation as described previously (**Pepeliaev et al., 2017**). Briefly, an enzyme (hya-luronan lyase from Streptococcus Pneumoniae, SpHyl, 10 µl) was added to the degradation solution removed from the degradation vessel and degraded for 30 min at 37 °C. The added amount of an enzyme was sufficient for complete total HA derivatives degradation to unsaturated native and modified HA disaccharides. HA derivatives were quantified from the respective calibration curve spectrophotometrically at 232 nm.

2.2.9. In-vitro cell viability

All the prepared nanofibrous layers were insoluble in aqueous environments. Their toxicity was tested using their extracts. Nanofibrous layers (100 mg) were immersed at a concentration of 1 mg/ml in Dulbecco's Modified Eagle Medium supplemented with 10% fetal bovine serum and extracted for 24 h (37 °C, 200 rpm shaking). The extracts were subsequently filtered (0.22 μm) and then used in the original concentration and after being diluted 2x, 10x, and 100x. 3 T3 cells were seeded one day before the experiment at a concentration of 3000 cells per well. The extracts were then applied in a volume of 200 il per well. A pure cultivation medium was used as the control. Viability was measured using the 3-(4,5-dimethylthiazol-2-yl)-2,5-diphenyl-tetrazo-lium bromide (MTT) assay. An MTT stock solution (20 µl; 5 mg/ml) was added to the cell culture medium in each well. The plates were incubated for 2.5 h at 37 °C. Subsequently, the MTT solution was removed, 220 µl of a lysis solution (IPA, 10% dimethylsulfoxide, 10% Triton x-100) was added, and lysis was performed for 30 min at room temperature and 150 rpm. Absorbance was read at 570 and 690 nm (A570 and A690, respectively) with an EnSight Multimode Plate Reader (Perki-nElmer). Data were processed in Kaleido (PerkinElmer). The final absorbance A was calculated according to the following equation:

$$A\ [-] = A570 - A690$$

The change in the viability of the treated cells was calculated relative to the control according to the following equation:

$$\text{Viability relative to control } [\%] = \left(\frac{A_{\text{sample}}}{A_{\text{control}}} - 1\right) \times 100$$

2.2.10. NHDF cell adhesion

For the cell (NHDF Normal Human Dermal Fibroblasts) adhesion the nanofibrous materials were cut into (1 x 1) cm^2 specimen and preincubated in partially heparinized blood from healthy donor. The samples were placed into microplate. Cells were stained with Dil stain. 30,000 cells were applied in a suspension to each well. Microplate were incubated at 37 °C, in 5% CO_2 for 24, 72 and 120 h. Cells were imaged with fluorescence microscope Nikon Eclipse-Ti. All measurements were made in three replicates.

2.2.11. Scratch assay (in vitro wound healing)

HaCaT cells (Human Immortalized Keratinocytes) were seeded onto Incucyte® Imagelock 96-well plate (45.000 cells per well in Dulbecco's Modified Eagle Medium (DMEM) supplemented with 10% fetal bovine serum) two days before the treatment. After 24 h of incubation (37 °C, 5% CO_2), the medium was changed to serum-free medium to stop the cell proliferation. The cells were serum-starved for 24 h (37 °C, 5% CO_2) (**Adeli et al., 2020**). All used nanofibrous materials were insoluble in aqueous environments and therefore, their effect on HaCaT cell migration was tested using only their extracts. Nanofibrous layers were immersed at a concentration of 1 mg/ml in serum-free DMEM and extracted for 24 h (37 °C, 200 rpm shaking). The extracts were subsequently filtered (0.22 μm) and then diluted to the concentrations 1000, 500, 100 and 10 μg/ml in a serum-free medium.

After 24 h serum-starving incubation, each well was rinsed with 1x phosphate buffered saline (PBS). The homogeneous and consistent wounds (700-800 im wide) were made using the Incucyte Wound-Maker. The WoundMaker was used to remove the cells to form cell-free zones, where the cells can migrate. The wells were rinsed again with 1 x PBS and with a serum-free medium. The extracts were then applied in a volume of 200 μl per well. Each sample at a defined concentration was tested in a quadruplet in at least three biological replicates. A cultivation medium with serum was used as a positive control (stimulates cell migration as well as proliferation) and medium without serum was used as a negative control. The cell migration was monitored by IncuCyte every 2 h for the total 48 h. Relative Wound Density (%; the density of cells in the wound area) was computed and expressed relative to the cell density outside of the wound area over time. Student's t-test was used to compare each sample with the positive and the negative control (at time 12, 24 and 48 h). A P-value < 0.05 was used to define a statistical significance.

3. Results and discussion

Each of the derivatives used in this study exhibits a different type of hydrophobization - L-HA carries a hydrophobic modification in its very structure, while F-HA becomes hydrophobic only after interacting with UV radiation. Electrospinning solutions of the individual derivatives can be prepared with different solvent systems, each suitable for one of the derivatives, but an electrospinning solution containing their combination has to be prepared using a single solvent system that is not 100% suitable for either of the two derivatives. When preparing electrospinning solutions containing L-HA, we had to take into consideration the natural hydrophobic properties of this material, which led us to select a solvent system composed mainly of IPA. Electrospinning solutions prepared with this system displayed good properties (dynamic viscosity, electrical conductivity, etc.); the spinning process was stable and the target yield of the spinning process was achieved. A relative humidity of 30-45% was maintained inside the spinning chamber. SEM images (**Fig. 2**) show that the prepared layers also contained some amount of fibers with very small diameters, the formation of which we attribute to the different natures of hydrophilic PEO (thinner fibers) and hydrophobic L-HA (thicker fibers). Due to its low degree of substitution, F-HA by itself is soluble in distilled water, which is why distilled water was used as the sole solvent to prepare F-HA-only solutions. A stable spinning process was achieved with solutions prepared in this way. The spinning of F-HA requires low relative humidity. The optimal level of relative humidity proved to be 10-15%. The prepared material was hydrophobized after the nanofibrous layers were spun and removed from the substrate. Images of the irradiated layers revealed no visible morphological changes (**Fig. 2**); from a macroscopic view, a slightly yellowish discoloration of the layers was apparent.

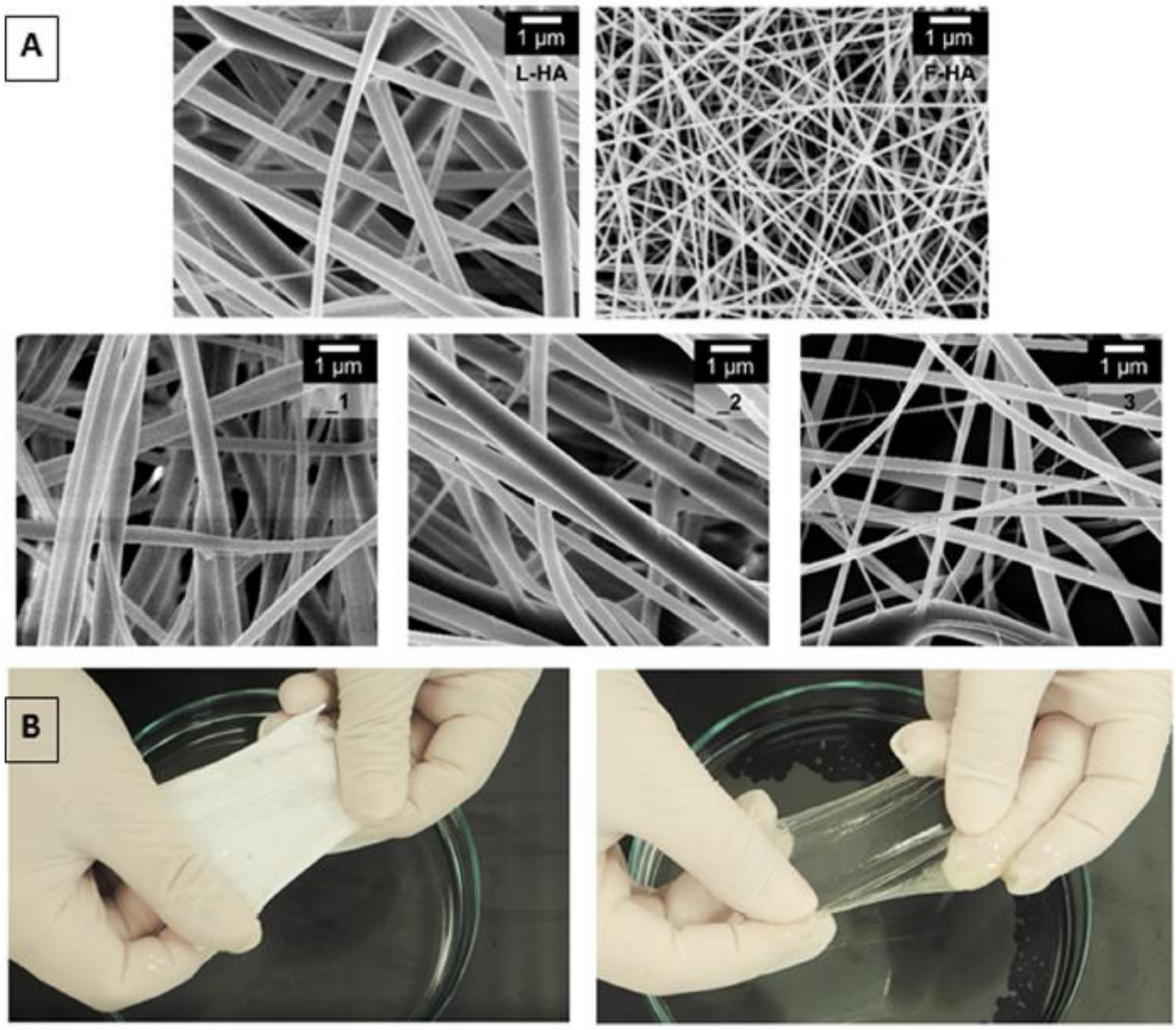

Fig. 2. (A) SEM images of fibrous structures of the prepared materials (_1 → L-HA/F-HA_1; _2 → L-HA/F-HA_2; _3 → L-HA/F-HA_3), (B) Appearance of nanofibrous materials after 5 min in PBS - L-HA (left), F-HA (right).

Considering that each of the two derivatives required a different solvent system, we expected that the solvent formula would need to be modified in order to allow the preparation of a solution containing their combination. However, the solvent system used for L-HA eventually also proved to be suitable for the preparation of composite solutions of L-HA and F-HA, even when the solute was composed mainly of F-HA. The two derivatives had slightly different requirements in relation to spinning process parameters, but the differences proved not to be a major issue and a stable spinning process was achieved.

The solvent system used for the preparation of a spinning solution evaporates during the electrostatic spinning process. If the spinning conditions are optimal, the solvent evaporates completely. We detected no traces of solvents in any of the samples of the prepared nanofibrous materials. None of the samples were treated in any way prior to their analysis (e.g. by being placed into a desiccator). The samples were stored under standard laboratory conditions.

F-HA fibers are naturally smaller in diameter than L-HA fibers. The fiber diameters of all the prepared composite materials ranged between the fiber diameters of the pure derivatives, indicating no undesirable material interactions. The nanofibrous material produced from the blend with the highest content of F-HA had the smallest fiber diameters of all the three composite materials. L-HA fibers

exhibited greater deviations from the average fiber diameter than F-HA fibers. As discussed above, the prepared L-HA layers also contained very thin fibers. A certain degree of inhomogeneity of a similar nature was also observed in composite materials containing a combination of L-HA and F-HA, and it was most pronounced in the L-HA/F-HA_3 material (**Fig. 2**, images _1 to _3). In all cases, this inhomogeneity was caused by the different degrees of affinity for water, exhibited by the individual polymers and using a less-than-ideal solvent system.

Despite the complications mentioned above, both polymers formed self-supporting fibrous layers with a weight-to-area ratio of around 10 g/m^2. Combining these two polymers did not result in any substantial changes in the yield of the spinning process, which was set up to run stably and continuously for the entire course of spinning even when using needleless emitters. Neither did we observe any major differences in the thicknesses of layers produced from the individual derivatives and from their blends (**Table 1**).

The prepared materials could be particularly used in applications that are required to withstand certain mechanical stress in environments with low as well as high levels of relative humidity. **Fig. 2**B shows what the materials produced from the individual derivatives look like after being hydrated (5 min in PBS).

Table 1 Average fiber diameter, thickness, and weight-to-area ratio of each material.

	Fiber diameter [nm]	Thickness [μm]	Weight-to-area ratio [g/m^2]
L-HA	659 ± 228	13.08 ± 3.21	9.30 ± 3.21
F-HA	127 ± 19	11.56 ± 2.39	6.77 ± 2.81
L-HA/F-HA_1	304 ± 106	15.77 ± 2.46	11.11 ± 1.29
L-HA/F-HA_2	479 ± 230	11.75 ± 0.89	7.29 ± 0.43
L-HA/F-HA_3	231 ± 95	16.94 ± 1.36	10.75 ± 1.11

While the material produced from L-HA retained its shape and mechanical properties for some time, the material produced from F-HA immediately turned transparent, became slightly compressed, and its mechanical properties changed - its extensibility increased. Combining these two derivatives makes it possible to produce various types of materials with different mechanical properties that can be tailored to the needs of the intended application.

Mechanical properties were evaluated in environments with different levels of relative humidity - 0%, 50%, and 95%. Observed changes in mechanical properties (**Fig. 3**) corresponded with the behavior of the individual materials described above. Also, comparing all studied combinations and pure materials, significant differences in their mechanical properties were observed before and after humidity increment. In an environment with a relative humidity of 0%, the strength values of the F-HA material samples were higher as expected, while the strength values of the L-HA material samples were the lowest. The strength values of F-HA were probably higher due to the presence of smaller-diameter fibers, which entangle with one another more during the spinning process. The mechanical properties of the composite materials in dry state corresponded with the different ratios of the individual polymers. This held true even at higher levels of relative humidity (50%), where all samples stress resistance generally doubly decreased, but the trending was maintained. Only in case of L-HA/F-HA_3, there was an approximately sevenfold decrease in the overall strength of the material. Increases in extensibility were observed both in the composite materials and in F-HA and L-HA. At 95% RH, the tensile strength of all materials decreased, which was caused by water molecules penetrating the fibrous structure and the structure becoming partially loose. Under these conditions, L-HA lost both strength and elasticity, and tore easily under mechanical stress. This behavior was also exhibited by

the composite material with the highest content of this derivative (L-HA/F-HA_1). Fibers in materials with a higher content of F-HA retained their strength and elasticity after being exposed to high levels of humidity better than fibers composed mainly of L-HA. They were weaker than dry fibers, but it was possible to handle the samples without damaging them - which is a key feature for all possible medical applications. With increasing relative humidity, F-HA became increasingly adhesive, which could be an issue when handling the material. In the L-HA/F-HA_2 and L-HA/F-HA_3 composites, this behavior was suppressed to a great degree by the presence of L-HA, which exhibits no such behavior, while the mechanical resistance of the materials was retained.

With increasing degree of relative humidity, the Young's modulus and Ultimate tensile strength naturally decreased (**Fig. 4**). In case of L-HA/F-HA_2 was reached the best compromise between stress resistance and elasticity, even in the highest degree of humidity. This material also, according to F-HA pure layer, showed the highest values of strain at breaking point of all three types of composites.

The derivatives used in this study differ not only in their mechanical properties but also in their microscopic structures. **Figs. 5 and 6** show SEM images of the prepared materials after their immersion in PBS (37 °C) for various periods of time: 1, 3, 8, 24, 48, and 72 h. The images clearly show that the material made from L-HA was not able to retain its fibrous structure for even 1 h of soaking in PBS; the fibers quickly became loose, pores disappeared, and a film is formed. The L-HA layers did retain some degree of porosity during the entire course of observation.

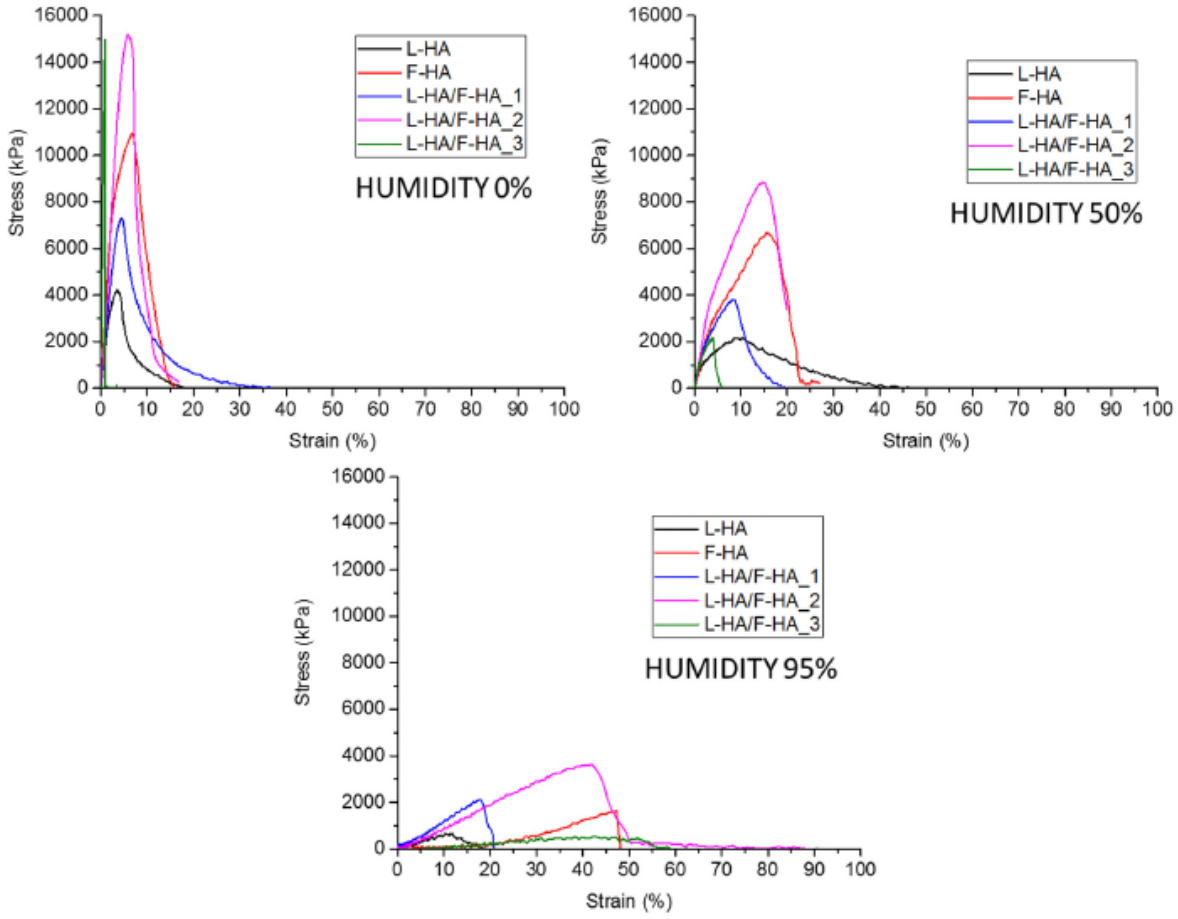

Fig. 3. Mechanical properties of the prepared materials in environments with different levels of RH - 0%, 50%, and 95%.

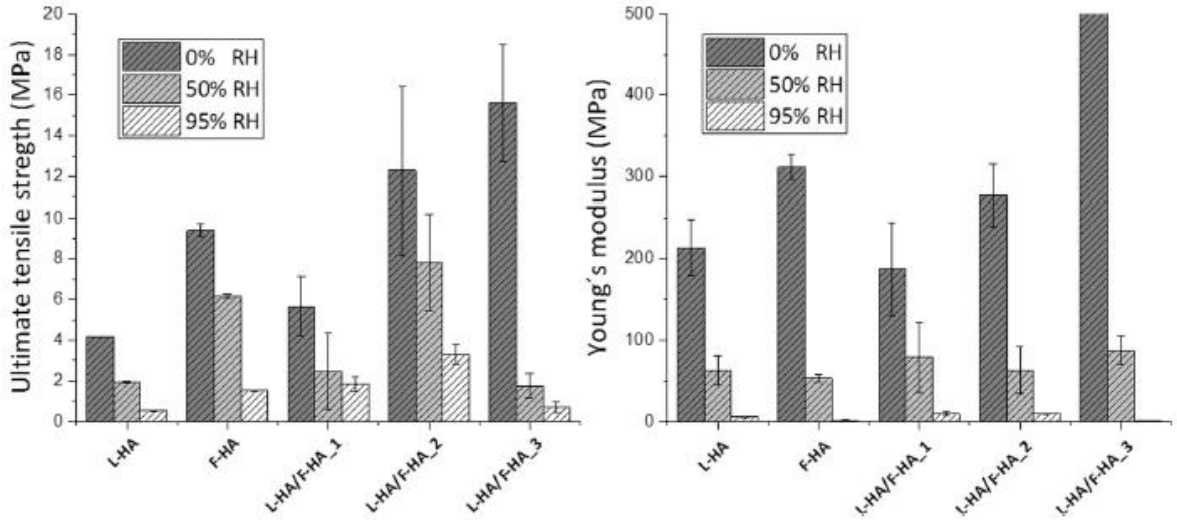

Fig. 4. Ultimate tensile strength and Young's modulus trending.

On the other hand, the material made from F-HA retained its fibrous structure for full 72 h and only minimal changes in fiber morphology were observed. Neither did we observe any major effect of PEO on the structure. PEO, present in the amount of 10% w/w, was not cross-linked in the structure or covalently bonded to it at all, and it can be therefore assumed that it washed out. Another fact indicating that PEO was being washed out is that the SEM images show areas where the fibers seem to slightly melt together. As the images were taken after the layers had dried again, these areas were probably formed mostly by PEO that had dried on the surface. The structures of composite materials changed with the changing ratio of L-HA and F-HA - the more F-HA a material contained, the more it retained its fibrous structure. After 72 h, only materials containing at least 48% w/w of F-HA retained their fibrous structure. The fibrous structure of these materials was only partially deformed by swelling, and there was only a moderate increase in their fiber diameters.

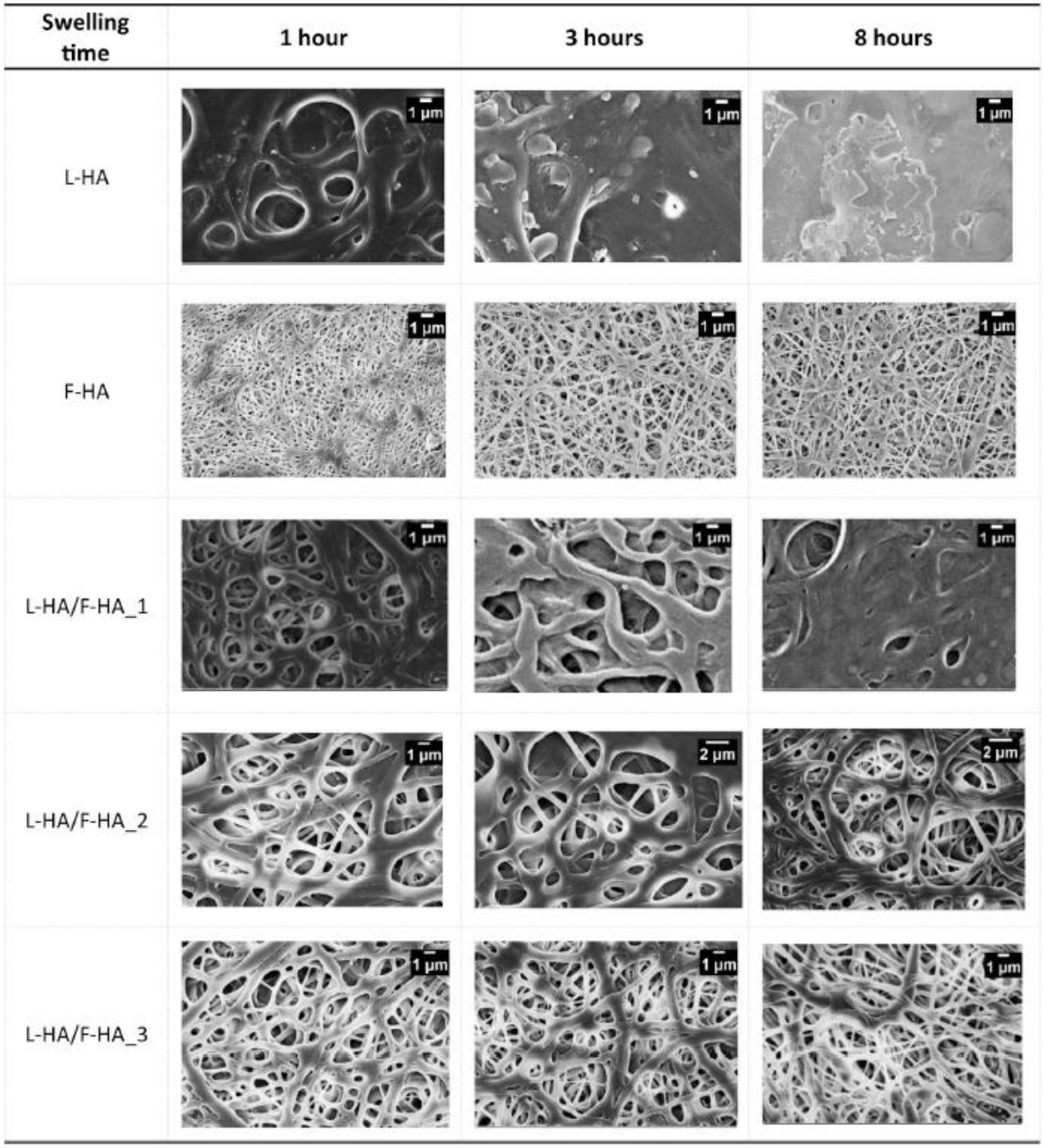

Fig. 5. Morphology of the prepared nanofibrous materials after 1, 3, and 8 h in PBS.

Further differences in the fibrous structure of the prepared materials were revealed by swelling tests. As mentioned above, upon their first contact with PBS, the individual materials exhibited different absorption behavior observable with the naked eye - layers produced from L-HA were not easily wettable and remained white after coming into contact with PBS (**Fig. 2**B), while layers produced from F-HA immediately absorbed the liquid into their structure and turned transparent (**Fig. 2**B). Important parameter, which affects the material's surface behavior is the type of hydrophobization. In our experimental section we used two different types - in F-HA nanofibers the hydrophobic feature of the material comes from chemical crosslinking, so some covalent bonds are made between the furyl-acrylic chains (so the natural hydrophilic property of HA is partially kept; the degree of substitution is low - about 5%, so there is a major part hydrophilic, but even though the covalent bonding is strong enough and homogeneously distributed in the layer to keep its fibrous form). Secondly, the L-HA

nanofibers are made from hydrophobically modified backbone of HA completely from the beginning (the degree of substitution is also higher than in F-HA - about 70%, so the material has much higher contact angle and lower wettability) and the ratio of hydrophilic non-modified HA is much lower. When it comes to contact with water environment, the F-HA layers macroscop-ically collide first - they turn transparent (visible in **Fig. 2**B) - but it's just an effect of the non-crosslinked part willingly binding water (the retraction of the layer), but the fibrous structure is still fixed, due to covalent crosslink. After the hydrophilic part is fully soaked, it partially swell (the expansion of the layer).

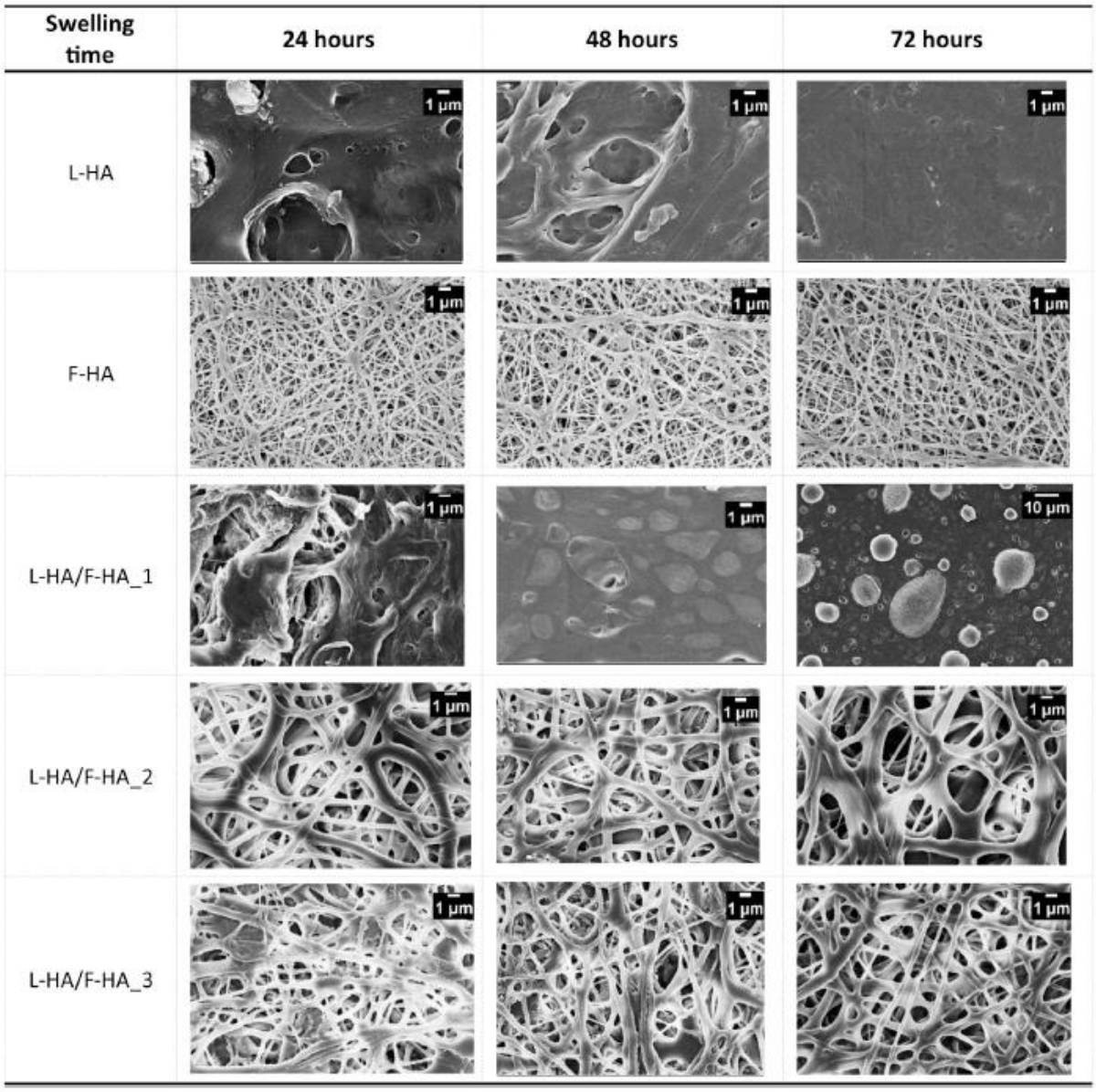

Fig. 6. Morphology of the prepared nanofibrous materials after 24, 48, and 72 h in PBS.

That's why the furyl HA derivative is taken as the keeper of fibrous structure. This material keeps its structure for days. Despite the L-HA sample, which is keeping its fibrous structure unchanged, for the first few minutes to 1 h (also the sample is not retracted) - it is caused by the time needed for the water drop to penetrate into the oily material surface - after that the fibers start to swell and the structure collides into non-porous film. This happens gradually through the whole layer, which also became transparent, after some time. But even when the fibrous structure in not fixed, the material keeps its mass and thickness. Also, partial minimal expansion of the sample occurs naturally as the water is being

soaked. When the composite layer is prepared, both discussed properties are applied. This makes the combined material unique.

There were no substantial changes in the volumes of composite samples during the entire course of their swelling. Composite layers containing both L-HA and F-HA behaved similarly to L-HA layers. After 8 h in PBS, all the layers were transparent. The L-HA material retained roughly its original shape even after 72 h of swelling and could still be handled without any issues. The swelling ratios of the L-HA samples were between 1000% and 2000% (**Fig. 7**); however, after accounting for standard deviation, the swelling ratios were comparable, which likely contributed to the ability of these samples to retain their shape as well as to their mechanical properties. The swelling ratios of these samples did not change over time. The fact that the samples lost their fibrous structure is one of the reasons to expect that a film would form and the number of pores would be reduced even after a single hour of soaking -there would be no space left to absorb the liquid into the structure anymore. The material produced from F-HA behaved differently in PBS. Immediately after getting in contact with PBS, its surface became wet, the material contracted and turned transparent (**Fig. 2**B), and its mechanical properties changed - it became very extensible. It remained in this form for the entire course of swelling. In its final form, the material therefore had a gelatinous consistency but at the same time retained its shape without any further visible contractions or expansions. The material absorbed large amounts of water into the pores between its fibers. This was reflected by the results of the swelling test, which showed that the swelling ratios increased over time (**Fig. 7**) and peaked after 48 h, by which time it can be expected the pores had become fully filled with water.

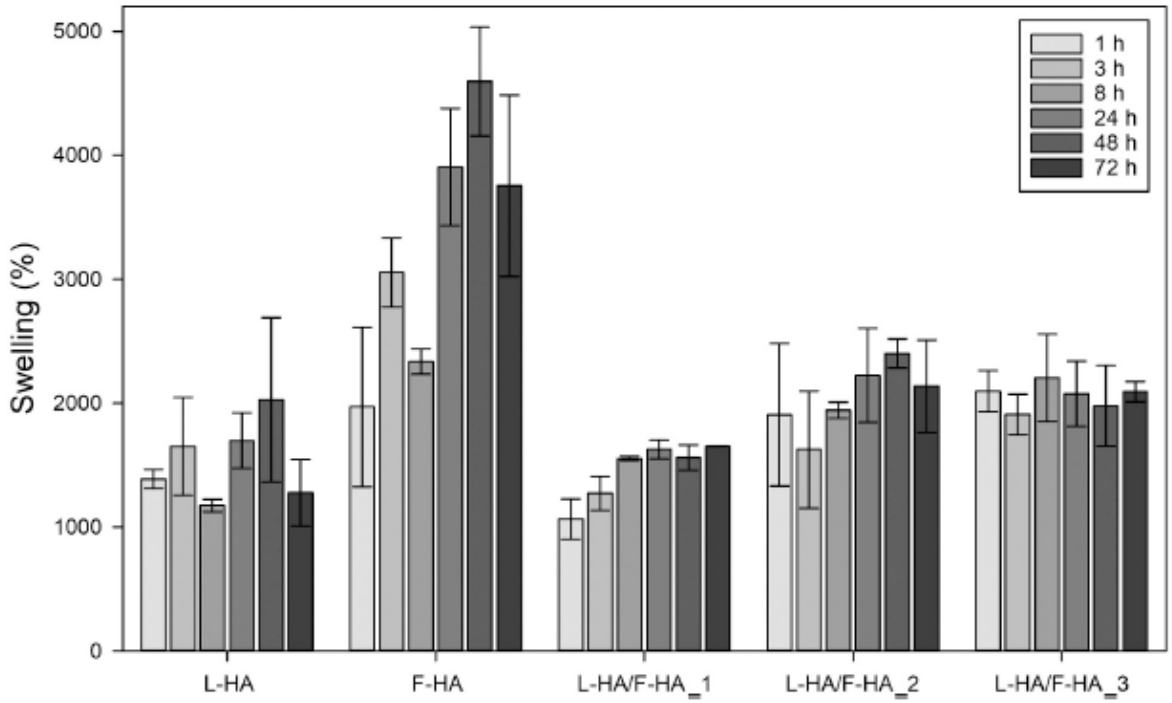

Fig. 7. Swelling behavior of nanofibrous materials at various swelling times.

The swelling ratios of composite materials and their behavior during swelling were similar to those of the material spun from L-HA, and this was true even for those materials that retained their fibrous structure during the entire course of swelling (L-HA/F-HA_2 and L-HA/ F-HA_3). The L-HA/F-HA_1 composite material exhibited virtually the same swelling ratios as the L-HA material (**Fig. 7**). The overall swelling ratios of the L-HA/F-HA_2 and L-HA/F-HA_3 composite materials were comparable, and they

were slightly higher than the swelling ratios of the L-HA and L-HA/F-HA_1 samples; surprisingly, there were no substantial changes in the ratios over time, despite the high porosity of the materials.

In vitro degradation experiments of various nanofibrous layers were performed in solution containing or not the HA hydrolase, namely BTH. Enzyme concentration was chosen to measure significant differences in degradation rates among samples studied and to complete the degradation in reasonable time. The degradation rates were calculated from the initial linear slope of Cumulative release (wt%) of HA derivatives versus time (**Fig. 8**). In general, cumulative releases of HA derivatives were more rapid in sodium acetate buffer containing BTH (compare **Fig. 8**A and B), i.e. L-HA and F-HA derivatives are both enzymatically degradable. The degradation rates generally decrease with increasing amount of L-HA derivative in the nanofibrous layer while the opposite is truth for F-HA. This behavior was caused by higher degree of substitution of L-HA derivative (DS 65-80%), so the F-HA (DS 5%) and its composites degradation rate was higher, because there was higher amount of non-modified HA. This trend wasn't affected with the presence or absence of BTH enzyme. The subsequent analysis of degradation products didn't show any potentially toxic or undesirable side substances. This degradability test showed, that due to the ability of F-HA derivative to willingly degrade, the best combination for any future medical applications, where is common presence of any physiological fluid, is to choose sample L-HA/F-HA_2 (red line in **Fig. 8**), because the degradation rate is not so high and the layer still keeps its fibrous structure at the same time (**Figs. 5 and 6**).

In vitro tests of cell viability were performed using extracts of nanofibrous layers produced from L-HA, F-HA, and the L-HA/F-HA_1, _2, and _3 blends.

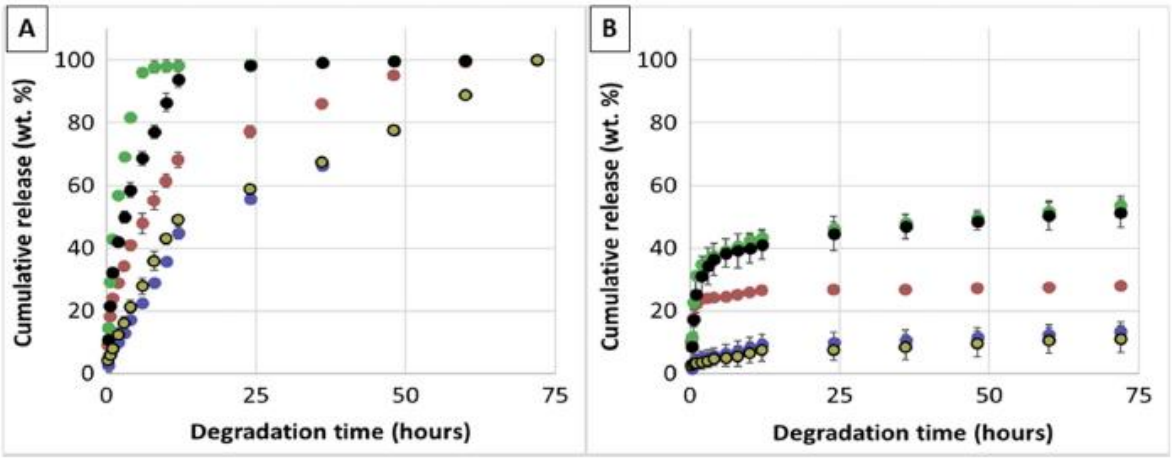

Fig. 8. Cumulative release of HA derivatives from nanofibrous layers. The degradation solution (0.01 M sodium acetate buffer pH 5.3 and 0.5 mg ml^{-1} BSA) contained 30 (A) or 0 (B) IU ml^{-1} of bovine testicular hyaluronidase. Sample L-HA/F-HA_1 is showed in blue, L-HA/F-HA_2 is showed in red, F-HA is showed in green, L-HA/F-HA_3 is showed in black and L-HA is showed in yellow. Error bars are the standard deviations of 3 replicates.

The results are shown in **Fig. 9**. Cell viability rates were evaluated relative to the controls. Positive values correspond to increases in cell proliferation and promotion of cell viability, while negative values correspond to inhibition of cell proliferation. As the data provided below demonstrated, extracts produced from L-HA-only layers promoted cell proliferation at all concentrations; the only case in which no positive effect was observed was when the extract was present in the sample in a concentration of 10 μg/ml, and even this sample promoted cell proliferation for the first 48 h. The cell viability diagram demonstrated that the UV-cross-linked FHA derivative did not promote cell proliferation as much as other materials containing LHA. Despite this sample showed only slight toxicity after 72 h. The L-HA/F-HA_1 composite material, which contained more L-HA than F-HA, also promoted

cell proliferation at all tested concentrations and measurement times; only samples with the highest concentration of 1000 μg/ml exhibited slight cell growth inhibition after 72 h, but only in lower concentrations. The extract of the L-HA/F-HA_2 composite layers, composed of equal parts of both derivatives, had mostly positive effect on cell proliferation at all concentrations. At the highest concentration, the extract of the L-HA/F-HA_3 composite material inhibited cell proliferation after 72 h from the beginning of the test. This effect can be attributed to the fact that the structure of the material was composed mostly of F-HA. Of all the tested materials, the one most suitable for potential direct contact with cell colonies therefore proved to be the composite material composed of equal parts of the two derivatives. Overall, none of the prepared nanofibrous materials can be evaluated as cytotoxic.

The NHDF cell adhesion tests were carried out to realize, if the nanofibrous samples are suitable for straight contact with mammalian tissue. The results (**Fig. 10**A) showed, that cells were not adhered to pure layers of L-HA and F-HA and also any positive cell proliferation in time was not visible. These layers were qualified as non-adherent. In case of F-HA, the non-adherent behavior was visible because of the high rate of degradability in the blood fluid, so the fibrous material slowly became gel-like and the cells were no longer capable of proliferating. The cells were just passively stuck in the gel. This behavior fully corresponds with data from cell viability tests (**Fig. 9**). Secondly, the L-HA layers showed similar results. Even though the degradation rate of this material is not as high, as in F-HA, the tendency of the material to make film in water-based environment, which was discussed with the swelling behavior above, is fast. Non-porous film structure also mechanically does not allow the prominent cell proliferation. The only samples, showing positive cell adhesion and proliferation in time, were L-HA/F-HA_2 and _3. As was demonstrated in enzymatic degradation part, the L-HA/F-HA composite with the same amount of both derivatives keeps approximately its fibrous structure and shape, so it works as a scaffold even in wet conditions. This result only confirms the previous statement about the suitability of the composite material for the future intended application.

The in vitro scratch wound healing assay is a convenient method to monitor effects of tested compounds on cell migration. The test of cell migration was performed using extracts of nanofibrous layers of L-HA, FHA, and the L-HA/F-HA_1, _2, and _3 blends. The results of cell migration are shown in **Fig. 10**B, C. The results show only a slight support of the migration of HaCaT cells. Neither a support of keratinocyte migration was observed, nor a negative influence of the extracts was detected. No statistically significant difference between the extracts and the control without serum was found. The positive control showed a statistically higher cell migration at time 48 h and in all concentrations compared to the tested compounds. These results are consistent with the observation, that the extracts from the tested materials are noncytotoxic. Although, we did not observe any direct support of cell migration in vitro, but there were also not any negative consequences caused by the presence of samples extracts straight to the HaCaT cells. Minimalized cell migration was probably supported by lower effect of the sample extract. The migration would be more significant, if the whole layers could be used, which was also visible during the cell adhesion tests. Nanofibrous materials from natural polymers provide generally great benefits when applied on a wound (such as keeping moist environment), that positively supports cell migration.

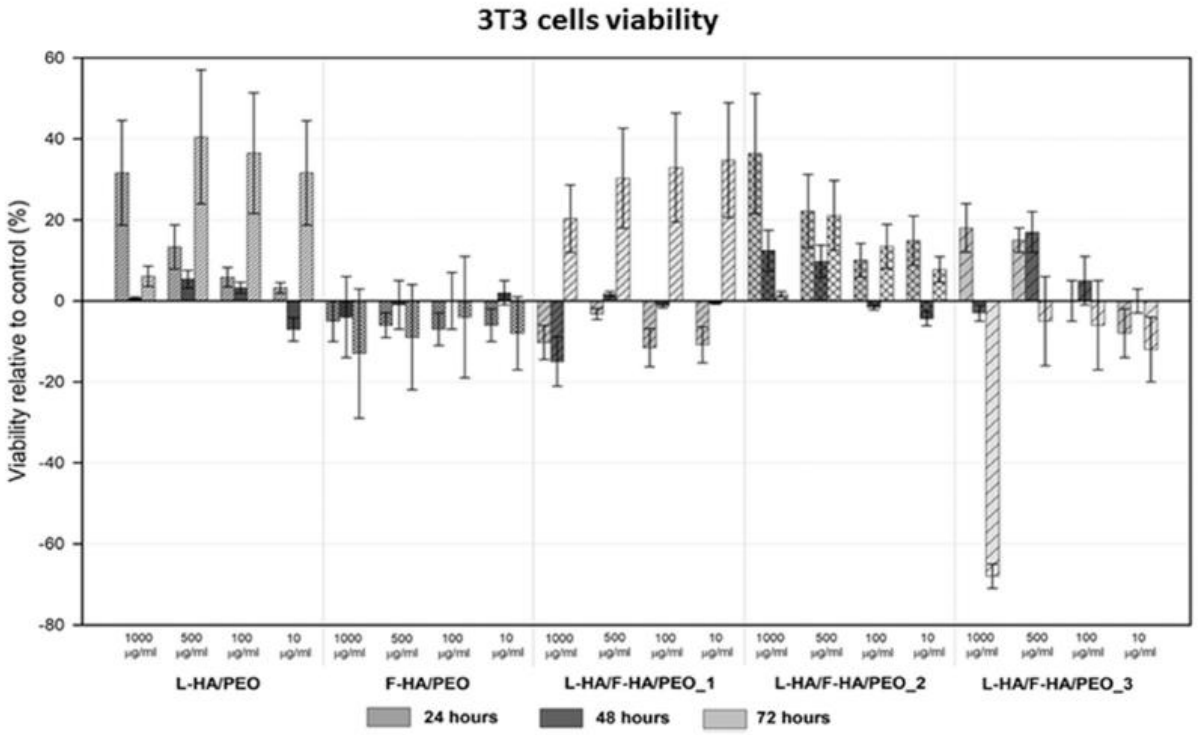

Fig. 9. Cell adhesion of NHDF cells on the L-HA/F-HA_2 and L-HA/F-HA_3.

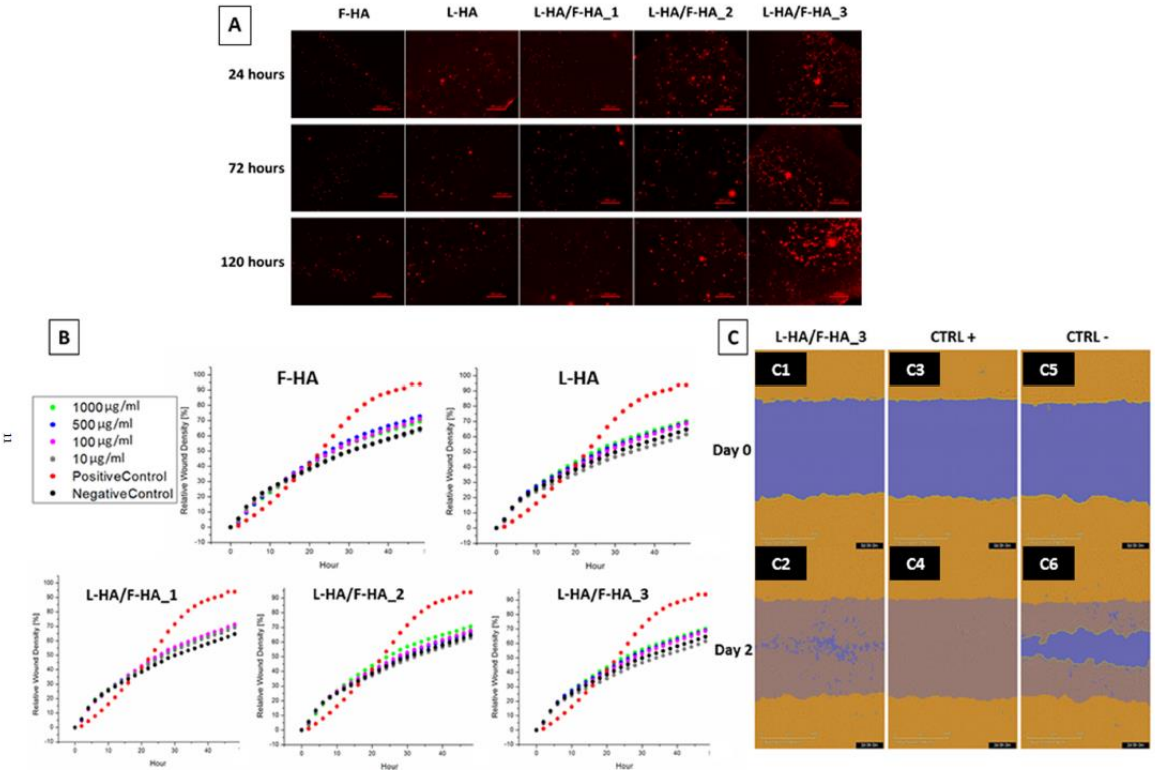

Fig. 10. Behavior of nanofibrous layers with physiological cell environment (A) Cell adhesion of NHDF cells with visible positive NHDF proliferation for samples L-HA/F-HA_2 and _3, (B),(C) Scratch wound healing assay (B) The curves show HaCaT cell migration (Relative Wound Density [%]) for the five tested compounds at the concentrations 1000 (green), 500 (blue), 100 (pink) and 10 (grey) pg/ml, positive control (red) and negative control (black) during 48 h. The values represent a mean of three independent replicates. Error bars representing SD were omitted to increase visual clarity of the data. (C) Representative images for L-HA/F-HA_3 at concentration 1000 µg/ml (C1, C2), positive (C3, C4) and negative control (C5, C6) with computational masks applied. The images show computational masks (yellow) of the detected cells over a blue area (the original scratches).

4. Conclusion

Self-supporting nanofibrous layers were prepared from two hydro-phobized derivatives of hyaluronic acid using the electrostatic spinning method. The layers were spun from individual derivatives and from blends containing different ratios of both derivatives. The prepared nanofibrous layers had no morphological defects and their fiber diameters ranged from 120 nm to 800 nm; the diameters of nanofibers produced from the UV-cross-linkable F-HA derivative were several times smaller than those of fibers produced from the derivative modified with residual lauric acid (L-HA). When spun individually, both materials displayed various positive and negative properties in relation to their mechanical resistance and stability in aqueous environments. For this reason, composite layers were prepared with the aim to eliminate their individual shortcomings. The composite nanofibrous layers exhibited increased extensibility while retaining enough tensile strength. The materials did not become deformed or significantly change their original size when exposed to aqueous environments nor did the layers turn into a gel after getting into contact with an aqueous medium. The layers were also able to retain a stable fibrous structure for 72 h. All the prepared nanofibrous materials were easy to handle even when wet. Neither the composite layers nor the layers prepared from the individual, unblended derivatives exhibited any undesirable cytotoxic behavior. The composites showed tendencies for cell adhesion support and demonstrated positive potential and environment for wound healing.

References

Adeli, H., Khorasani, M., & Parvazinia, M. (2020). Wound dressing based on electrospun PVA/chitosan/starch nanofibrous mats: Fabrication, antibacterial and cytocompatibility evaluation and in vitro healing assay. 2019(122), 238-254. **https://doi.org/10.1016/j.ijbiomac.2018.10.115**

Almasian, A., Najafi, F., Eftekhari, M., Ardekani, M. R. S., Sharifzadeh, M., & Khanavi, M. (2020). Polyurethane/carboxymethylcellulose nanofibers containing Malva sylvestris extract for healing diabetic wounds: Preparation, characterization, in vitro and in vivo studies. 2020(114), Article 111039. **https://doi.org/10.1016/). msec.2020.111039**

Bobula, T., Betak, J., Buffa, R., Moravcova, M., Klein, P., Zidek, O., Chadimova, V., Pospisil, R., & Velebny, V. (n.d.). Solid-state photocrosslinking of hyaluronan microfibres. 2015(125), 153-160. doi:10.1016/j.carbpol.2015.02.027.

Chmelar, J., Mrazek, J., Hermannova, M., Kubala, L., Ambrozova, G., Kocurkova, A., Drmota, T., Nesporova, K., Grusova, L., & Velebny, V. (2019). Biodegradable freestanding films from lauroyl derivatives of hyaluronan.. 2019(224). **https://doi.org/ 10.1016/j.carbpol.2019.115162**

Collins, M. N., & Birkinshaw, C. (2007a). Comparison of the effectiveness of four different crosslinking agents with hyaluronic acid hydrogel films for tissue-culture applications. 2007(104), 3183-3191. **https://doi.org/10.1002/app.25993**

Collins, M. N., & Birkinshaw, C. (2008b). Investigation of the swelling behavior of crosslinked hyaluronic acid films and hydrogels produced using homogeneous reactions. 2008(109), 923-931. **https://doi.org/10.1002/app.27631**

Creuzet, C., Kadi, S., Rinaudo, M., & Auzaly-Velty, R. (2006). In , 2006 (47). New associative systems based on alkylated hyaluronic acid. Synthesis and aqueous solution properties (pp. 2706-2713). **https://doi.org/10.1016/j.polymer.2006.02.052**

Debels, H., & Hamdi, M. (2015). Dermal matrices and bioengineered skin substitutes: A critical review of current options. 2015 (10). **https://doi.org/10.1097/ G0X.0000000000000219** (n.d.).

Dicker, K. T., Gurski, L. A., Pradhan-Bhatt, S., Witt, R. L., Farach-Carson, M. C., & Jia, X. (2014). Hyaluronan: A simple polysaccharide with diverse biological functions. Acta Biomaeralia, 10, 1558-1570. **https://doi.org/10.1016Zj.actbio.2013.12.019**

Dvorakova, J., Kucera, L., Kucera, J., Svik, K., Foglarova, M., Muthný, T., Pravda, M., Nemcova, V., Velebny, V., & Kubala, L. (n.d.). Chondrogenic differentiation of mesenchymal stem cells in a hydrogel system based on an enzymatically crosslinked tyramine derivative of hyaluronan: Chondrogenic Differentiation of MSC in a Hydrogel System. 2014(102), 3523-3530. doi:10.1002/jbm.a.35033.

Eenschooten, C., Vaccaro, A., Delie, F., Guillaumie, F., T0mmeraas, K.,Kontogeorgis, G. M., Schwach-Abdellaoui, K., Borkovec, M., & Gurny, R. (2012). Novel self-associative and multiphasic nanostructured soft carriers based on amphiphilic hyaluronic acid derivatives. 2012(87), 444-451. **https://doi.org/ 10.1016/j.carbpol.2011.08.004**

Fang, Y., Zhu, X., Wang, N., Zhang, X., Yang, D., Nie, J., & Ma, G. (2019). Biodegradable core-shell electrospun nanofibers based on PLA and y-PGA for wound healing. 2019 (116), 30-37. **https://doi.org/10.1016/j.eurpolymj.2019.03.050**

Finelli, I., Chiessi, E., Oddo, L., Galesso, D., Renier, D., & Paradossi, G. (2014). Collective dynamics and transient behavior of partially hydrophobic hyaluronic acid chains. 2014(215), 140-147. **https://doi.org/10.1002/macp.201300503**

He, J., Liang, Y., Shi, M., & Guo, B. (2020). Anti-oxidant electroactive and antibacterial nanofibrous wound dressings based on poly(e-caprolactone)/quaternized chitosan-graft-polyaniline for full-thickness skin wound healing. 2020(385), Article 123464. **https://doi.org/10.1016/j.cej.2019.123464**

Huerta-Angeles, G., Bobek, M., Prikopova, E., Smejkalova, D., & Velebny, V. (2014). Novel synthetic method for the preparation of amphiphilic hyaluronan by means of aliphatic aromatic anhydrides. 2014(111), 883-891. **https://doi.org/10.1016/j. carbpol.2014.05.035**

Huerta-Angeles, G., Brandejsova, M., Knotkova, K., Hermannova, M., Moravcova, M., Smejkalova, D., & Velebny, V. (2016). Synthesis of photo-crosslinkable hyaluronan with tailored degree of substitution suitable for production of water resistant nanofibers. 2016(137), 255-263. **https://doi.org/10.1016/j.carbpol.2015.10.077**

Liu, Y., Zhou, S., Gao, Y., & Zhai, Y. (2019). Electrospun nanofibers as a wound dressing for treating diabetic foot ulcer. 2019(14), 130-143. **https://doi.org/10.1016/j. ajps.2018.04.004**

Longinotti, C. (2014). The use of hyaluronic acid based dressings to treat burns: A review. Burns & Trauma, 2(4), 162-168.

Miguel, S. P., Figueira, D. R., Simoes, D., Ribeiro, M. P., Coutinho, P., Ferreira, P., & Correia, I. J. (2018). In , 2018 (169). Electrospun polymeric nanofibres as wound dressings: A review (pp. 60-71). **https://doi.org/10.1016/j.colsurfb.2018.05.011**

Necas, J., Bartosikova, L., Brauner, P., & Kolar, J. (2008). Hyaluronic acid (hyaluronan): a review. Veterinarni Medicina, 53, 397-411. **https://doi.org/10.17221/1930-VETMED**

Pepeliaev, S., Hrudikova, R., Jilkova, J., Pavlik, J., Smirnou, D., Cerny, Z., & Franke, L. (2017). Colorimetric enzyme-coupled assay for hyaluronic acid determination in complex samples. European Polymer Journal, 2017(94), 460-470. **https://doi.org/ 10.1016/j.eurpolymj.2017.07.036**

Sill, T. J., & von Recum, H. A. (n.d.). Electrospinning: Applications in drug delivery and tissue engineering. 2008(29), 1989-2006. doi:10.1016/j.biomaterials.2008.01.011.

Smejkalova, D., Hermannova, M., Sulakova, R., Prusova, A., Kucerik, J., & Velebny, V. (2012). In , 2012 (87). Structural and conformational differences of acylated hyaluronan modified in protic and aprotic solvent system (pp. 1460-1466). **https://doi.org/ 10.1016/j.carbpol.2011.09.057**

Snetkov, P., Morozkina, S., Uspenskaya, M., & Olekhnovich, R. (n.d.). Hyaluronan-Based Nanofibers: Fabrication, Characterization and Application. 2019(11), 2036. doi: 10.3390/polym11122036.

Unalan, I., Endlein, S. J., Slavik, B., Buettner, A., Goldmann, W. H., Detsch, R., & Boccaccini, A. R. (2019). Evaluation of electrospun poly(e-caprolactone)/gelatin nanofiber mats containing clove essential oil for antibacterial wound dressing. 2019 (11), 570. **https://doi.org/10.3390/pharmaceutics11110570**

Vercruysse, K. P., Marecak, D. M., Marecek, J. F., & Prestwich, G. D. (n.d.). Synthesis and in Vitro Degradation of New Polyvalent Hydrazide Cross-Linked Hydrogels of Hyaluronic Acid. 1997(8), 686-694. doi:10.1021/bc9701095.